Influence of Background Divergent Moisture Flux on the Frequency of North Pacific Atmospheric Rivers

SAMSON HAGOS,[a] L. RUBY LEUNG,[a] OLUWAYEMI GARUBA,[a] CHRISTINA M. PATRICOLA[b,c]

[a] *Pacific Northwest National Laboratory, Richland, Washington*
[b] *Iowa State University, Ames, Iowa*
[c] *Lawrence Berkeley National Laboratory, Berkeley, California*

(Manuscript received 20 January 2021, in final form 28 April 2021)

ABSTRACT: The frequency of North Pacific atmospheric rivers (ARs) affects water supply and flood risk over western North America. Thus, understanding factors that affect the variability of landfalling AR frequency is of scientific and societal importance. This study aims at identifying the sources of the moisture for North Pacific ARs and assessing how different modes of variability modulate these sources. To this end, the sources and variability of the background divergent component of the integrated moisture flux (DIVT) in ARs are identified using MERRA reanalysis. It is shown that in the boreal winter, this background DIVT in ARs is related to the outflow from the subsidence over the subtropics that transports moisture northward, while in summer it is related to the Asian monsoon and it transports moisture northwestward. This leads to a seasonal northwest–southeast movement of the AR frequency climatology. At the intraseasonal scale, propagation of the Madden–Julian oscillation introduces an anticlockwise rotation of the background DIVT, with northward transport in phases 1 and 2, westward in 3 and 4, southward in 5 and 6, and eastward in 7 and 8, making landfall over the west coast of North America most likely during the last two phases. Similarly, El Niño–Southern Oscillation variability also affects the frequency of ARs through modulation of the westerly background DIVT, favoring landfall over the U.S. West Coast during strong El Niño phases. It is shown that in general the likelihood of AR landfall over the western United States is correlated with the zonal background DIVT over northeastern Pacific.

KEYWORDS: Extreme events; Madden–Julian oscillation; ENSO; Seasonal variability

1. Introduction

Atmospheric rivers, narrow corridors of moisture flux that can stretch over thousands of kilometers, are key components of the hydrological cycle of western North America both in their role in alleviating droughts as well as in potentially causing severe floods (Zhu and Newell 1998; Ralph et al. 2006; Leung and Qian 2009). They are estimated to supply 30%–50% of precipitation over the West Coast of the United States (Dettinger et al. 2011; Rutz et al. 2014), with 33%–74% of droughts estimated to have ended by the arrival of atmospheric rivers (ARs; Dettinger 2013). ARs can also cause extreme coastal winds and significant damage (Waliser and Guan 2017). Given their importance, there has been an extensive body of research on the relationship of the variability of AR frequency with the large-scale environment. In general, these investigations followed two complementary paths, with the first focusing on circulation patterns associated with known modes of variability and their projections onto and modulation of ARs and the other aiming to understand the moisture sources of ARs and how they vary.

The first line of inquiry includes a study by Guan et al. (2012) and Guan and Waliser (2015) that documented the relationship between teleconnection patterns relating the Madden–Julian oscillation (MJO) and AR-related snowpack over Sierra Nevada. Similar studies have been expanded to other modes of variability more recently by several authors. For example, Ryoo et al. (2013) and Payne and Magnusdottir (2014) performed similar analyses and found that in a composite sense the eastward progression of ARs over the Pacific Ocean follows the jet, Rossby wave propagation, and anticyclonic Rossby wave breaking in the upper troposphere. These studies suggest a role for El Niño–Southern Oscillation (ENSO) in modulating AR landfall, with El Niño favoring a relatively strong subtropical jet, and the enhanced cyclonic wave breaking enhances zonal moisture transport to the western United States. Mundhenk et al. (2016) analyzed the seasonal variability of AR frequency, ENSO, the MJO, and their interactions using Modern-Era Retrospective Analysis for Research and Applications (MERRA) reanalysis. They found that ARs exist throughout the year over the North Pacific and shift northwestward (southeastward) during boreal summer (winter). They also showed that ENSO and the MJO may strengthen or weaken the seasonal cycle of AR activity, but noted that this effect on AR frequency varies greatly with location. Guirguis et al. (2018) found that AR landfall along the U.S. West Coast is largely associated with the superposition of a couple of modes of atmospheric variability. They showed that the circulation patterns that arise from the superposition steer moisture plumes up and down the western coast of North America. Furthermore Gershunov et al. (2017) demonstrated a role for Pacific decadal variability in the rising trend of landfalling AR activity.

Denotes content that is immediately available upon publication as open access.

Supplemental information related to this paper is available at the Journals Online website: https://doi.org/10.1175/JCLI-D-21-0058.s1.

Corresponding author: Samson Hagos, samson.hagos@pnnl.gov

DOI: 10.1175/JCLI-D-21-0058.1

The second line of investigation, which can be thought of as a Lagrangian perspective, focuses on understanding the formation and life cycle of ARs in general and the variability in their moisture source (e.g., Zhou et al. 2018; Neiman et al. 2008). Several studies from such a perspective emphasized the role of local moisture supply to ARs in contrast to the remote tropical sources that their long filamentary characteristics suggest. Bao et al. (2006) argued that ARs represent not the trajectory of moisture but rather the instantaneous position of enhanced moisture. In a similar way, Sodemann and Stohl (2013) and Dacre et al. (2015) highlighted the role of local moisture sources associated with the leading edges of cold fronts and their potential contribution to the formation and maintenance of ARs.

An important gap in our understanding of ARs is related to their place in the total moisture transport. Examination of that may lead to deeper insight into the source of their moisture and may provide physical explanations for the well-documented variability in their frequency and spatial distribution discussed above. Since the total moisture transport and its variabilities are related to the constraints imposed by energy input to the atmosphere, one can hypothesize that monsoonal as well as ENSO and MJO related variations in moisture transport would be reflected in the availability of moisture for ARs. In this work we consider this hypothesis. Specifically we aim to 1) identify the sources of the moisture for North Pacific ARs, 2) examine how different modes of variability modulate these sources, and 3) examine the impacts of these modes of variability on the spatial distribution of AR frequency and the implications for the likelihood of ARs making landfall over the United States. To this end we take a hybrid of the two perspectives discussed above as we investigate the spatial distribution of ARs in the context of the total zonal and meridional moisture transport and their variability as part of the global water cycle.

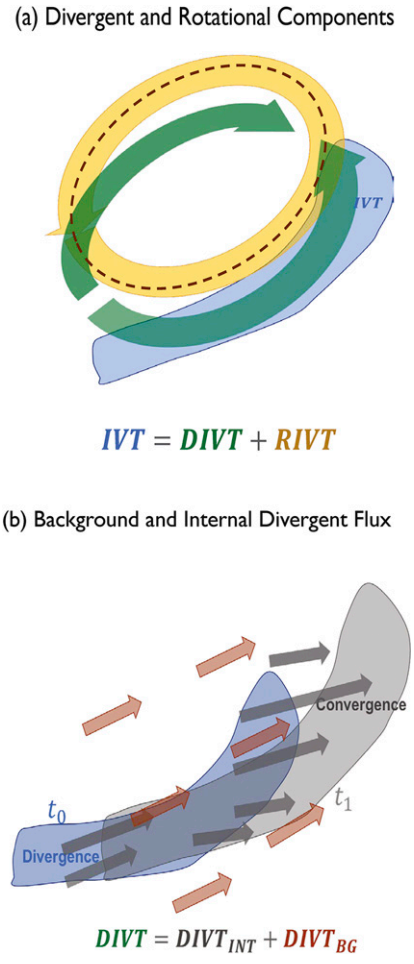

FIG. 1. (a) A conceptual model of an AR event as a contiguous area of IVT exceeding a threshold value and the partitioning of the IVT into divergent and rotational components. The dashed line marks the closed loop of constant moisture flux potential (i.e., net flux by rotational component is zero). (b) Further partition of the DIVT into the background and that associated with the divergence field within the ARs.

2. Data and method

a. Data

This work makes use of 38 years of (1980–2017) 3-hourly AR mask obtained using the TEMPEST tracking algorithm developed by Ullrich and Zarzycki (2017) archived by the Atmospheric River Tracking Method Intercomparison Project (ARTMIP; Shield et al. 2018). The algorithm identifies objects north of 15°N with integrated vapor transport (IVT) $>$ 250 kg $m^{-1} s^{-1}$ and size greater than 120 000 km^2 in the MERRA, version 2 (MERRA-2), reanalysis. While there is a significant sensitivity of AR frequency metric to AR tracking algorithm as documented in Rutz et al. (2019), TEMPEST is selected because it lies in the middle range in terms of both frequency and landfall count for western North America (see Fig. 6 and Rutz et al. 2019). We also use the corresponding 38 years of MERRA2 IVT.

The Wheeler and Hendon (2004) Real-Time Multivariate MJO index (RMM) is used to define MJO phases. The ENSO longitude index (ELI) developed by Williams and Patricola (2018) is used to define the ENSO phases. This index represents the average longitude of deep convection and therefore the centers of tropical Pacific convergence that is most relevant to this study. Following Williams and Patricola (2018), La Niña is defined as ELI $<$ 150°E, Neutral for ELI between 150° and 160°E, El Niño Modoki for ELI within the range of 160°–175°E, strong El Niño for ELI within the range of 175°–185°E and extreme El Niño for ELI $>$ 185°E.

b. Method: A conceptual model of ARs

ARs are generally defined as contiguous objects with IVT exceeding a certain threshold, typically 250 kg $m^{-1} s^{-1}$, and meeting a specific geometric criterion of length and width. According to the Helmholtz decomposition theorem, given the IVT vector field in a given AR object, one can define a closed area and the divergent and rotational components of the IVT such that the net moisture transport across the closed loop is accomplished by only the divergent component. Figure 1a

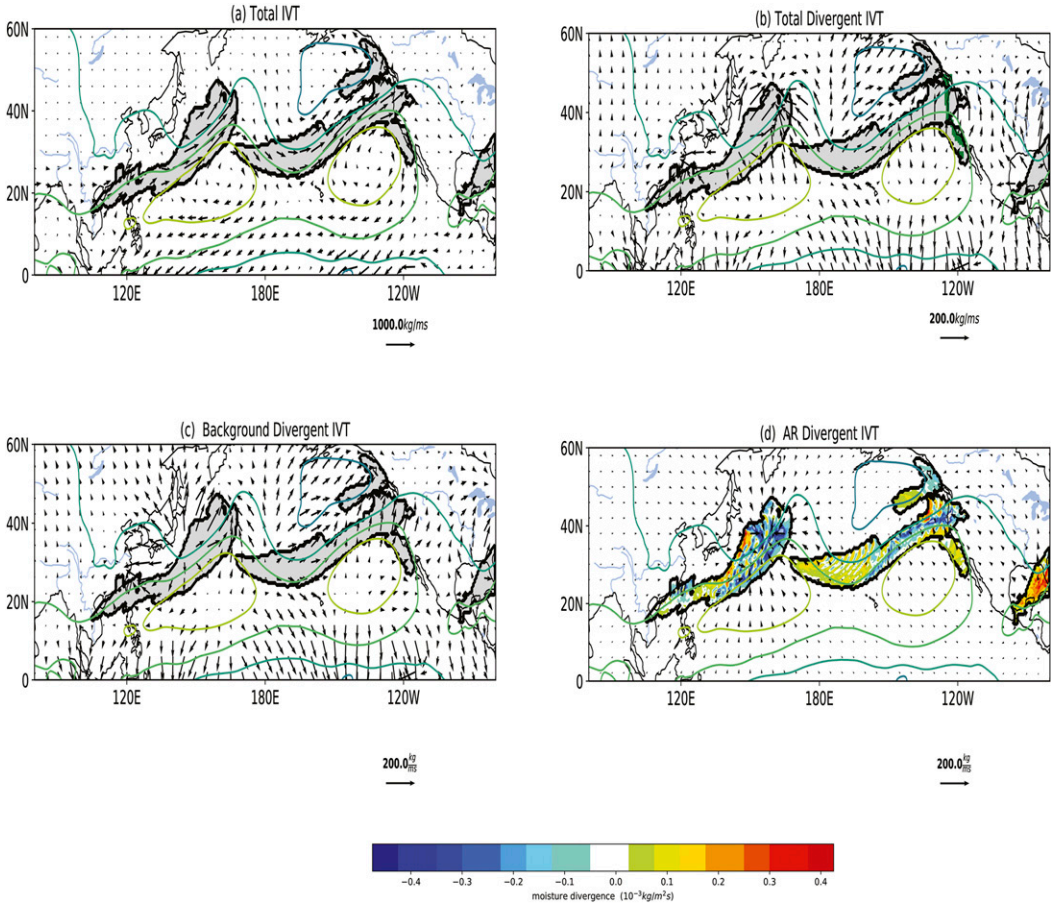

FIG. 2. An example of AR objects (shading) and (a) associated IVT (arrows), (b) the divergent component of the IVT (arrows), (c) the background (arrows), and (d) the internal AR parts of the total DIVT (arrows). In (d), the moisture divergence field is shown in shading.

shows a schematic of such decomposition. While the divergent component transports moisture from one side of the loop to the other, the rotational component represents the channeling of the moisture flux within the narrow corridor with zero net transport across the closed area.

The divergent IVT (DIVT) is nonlocally related to the moisture flux divergence (δ hereafter) in that DIVT within the AR under consideration is related to the divergence field everywhere on the globe and therefore a vector sum of contributions from the δ fields inside and outside the AR. The latter (δ) corresponds to the background transport required to balance the precipitation and evaporation around the globe but happens to be within the object defined as an AR and therefore contributes to the total IVT meeting the required IVT threshold used in the definition of AR. To understand the former (DIVT within the AR), consider a pair of consecutive snapshots of IVT associated with an AR event. The areas where the two snapshots do not overlap form a pair of areas of divergence and convergence (Fig. 1b). Changes in the shape of the IVT due to entrainment and detrainment of vapor and momentum would also be reflected in the difference divergence fields between successive snapshots. Below we present the practical approach of partitioning the total IVT of AR into rotational and divergent components and further partition the latter into internal and background components associated with the divergence fields within and outside the AR objects respectively.

First, the global daily moisture flux divergence (δ) is calculated by taking the divergence of IVT:

$$\delta = \nabla \cdot (\mathrm{IVT}). \tag{1}$$

The moisture flux potential φ is then calculated by solving the Poisson equation:

$$\nabla^2(\varphi) = \delta. \tag{2}$$

From the moisture flux potential, the total divergent IVT is obtained by taking the gradient of φ:

$$\mathrm{DIVT} = \nabla \cdot (\varphi). \tag{3}$$

To calculate the divergent IVT that is internal to ARs, a new moisture flux divergence field is defined by using the AR mask as follows:

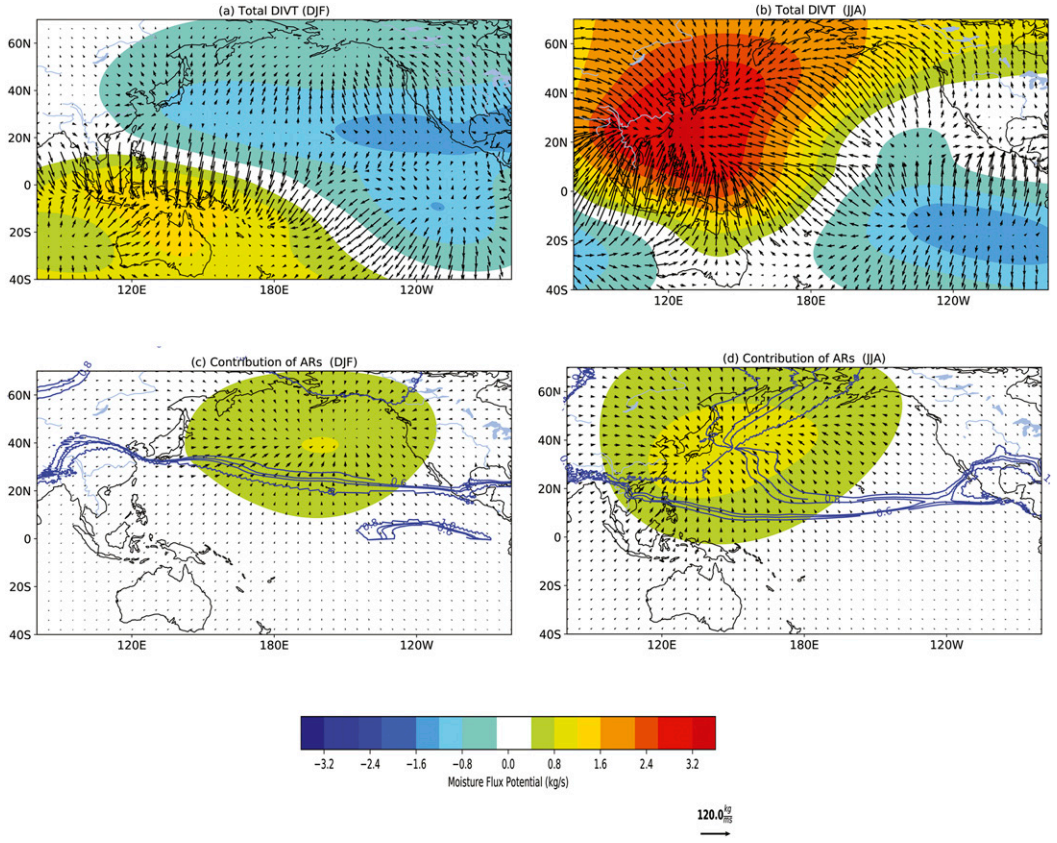

FIG. 3. Total DIVT (arrows) and moisture flux potential (shading) in boreal (a) winter and (b) summer. (c),(d) The corresponding contributions of ARs. The contours represent the fractional contribution of ARs to the total meridional DIVT. Only the 0.6, 0.8, and 1.0 contours are shown.

$$\nabla^2(\varphi_{\mathrm{INT}}) = \delta_{\mathrm{INT}}, \quad \text{where} \quad \delta_{\mathrm{INT}} = \begin{cases} \delta & \text{if} \quad \text{AR mask} = 1 \\ 0.0 & \text{if} \quad \text{AR mask} = 0 \end{cases}, \tag{4}$$

from which

$$\mathrm{DIVT}_{\mathrm{INT}} = \nabla \cdot (\varphi_{\mathrm{INT}}). \tag{5}$$

Finally, the background divergent IVT is defined as

$$\mathrm{DIVT}_{\mathrm{BG}} = \mathrm{DIVT} - \mathrm{DIVT}_{\mathrm{INT}}. \tag{6}$$

An example of the above procedure is provided in Fig. 2, which shows a snapshot of an arbitrarily selected pair of AR events. The total IVT at the time of the snapshot is shown in Fig. 2a (arrows) while the divergent component (DIVT) is shown in Fig. 2b. In the latter, the divergent flux comprises of both fluxes along the length of the AR as well as those associated with fluxes that originate from the anticyclones ahead of the AR events, transporting moisture to the cyclones northwest of the anticyclones, thereby crossing the AR objects. As shown in Fig. 2c much of the divergent flux crossing the AR objects is part of the background flow. The actual divergent moisture flux internal to the ARs is relatively small. The divergence and convergence pair associated with the movement of ARs (Fig. 2d), discussed in the conceptual model (Fig. 1b) are depicted by the shadings. Thus, from the definition, ARs can be considered as a channeling of the background DIVT into narrow filaments. This channeling is accomplished by the nondivergence component that is primarily associated with synoptic disturbances while the background DIVT is part of the global hydrological cycle. The sources and sinks of this background DIVT, its intraseasonal and interannual variability and its influence on AR frequency are the subjects of the sections to follow. However, it is worth noting that this method of identifying moisture sources and sinks is equivalent to Lagrangian tracking but for the whole moisture field instead of for predefined objects. For example, if one considers the moisture budget equation, setting temporal variability, evaporation, and precipitation aside, $dq/dt = -\mathbf{r}(d/dr) \cdot (\mathbf{v}q)$. The left-hand side represents the Lagrangian perspective, while the right-hand side represents the moisture divergence perspective. Our analysis amounts to calculating the unit vector $\mathbf{r}$ along which moisture is transported. Note that $\mathbf{r}$ is the direction of moisture transport and is perpendicular to the constant moisture flux potential contours as will be further discussed below. A closed contour of moisture flux potential represents the source or sink depending on the direction of $\mathbf{r}$.

3. Seasonal, subseasonal, and interannual variability

a. Total moisture transport and the contributions of ARs

Consider the climatology of the total divergent circulation. Figure 3 shows the total divergent moisture flux (arrows) and moisture flux potential during winter (DJF) and summer (JJA). As expected, the total divergent moisture flux corresponds to the Australian and Asian monsoon systems in DJF and JJA, respectively. In both seasons, there is a poleward transport of moisture over northern Pacific but for entirely different reasons between the seasons. In boreal winter, the poleward flux is related to the outflow from the subsidence over the subtropics. In boreal summer, on the other hand, the poleward flux is an extension of the Asian monsoon. One key difference between these two seasons is that, in boreal winter the moisture flux is southerly while in boreal summer it is southeasterly. The contributions of ARs are shown in Figs. 3c and 3d. The first thing to notice is that the moisture convergence associated with ARs reflects the seasonality of the total DIVT, southerly in winter and southeasterly in summer. The contribution of ARs to the meridional DIVT is shown in contours. While the AR-contributed meridional DIVT varies significantly regionally, ARs contribute between 60% and 100% of the total meridional DIVT at some latitudes.

b. Seasonality of AR frequency

Now that we have shown the seasonality of total moisture transport and that a significant portion of it is accomplished by ARs, it follows from the definition of ARs that their frequency is modulated by the seasonality of the background moisture flux. Figure 4 shows the seasonal mean AR frequency overlaid on the background divergent moisture flux ($DIVT_{BG}$), which is a component of the AR IVT as discussed in the last section. The samples of 38 years of annual climatologies and seasonal anomalies are used to test statistical significance of the latter using Student's *t* test as the samples are independent. Only AR frequency anomalies that are statistically significant at the 95% confidence level are shaded. In comparison to their annual mean climatology (the red contours), ARs in boreal winter extend farther southeast with the stronger background divergent flux originating from the subtropical high over eastern Pacific (Fig. 4a). In boreal summer the background flow is southeasterly as the Asian monsoon introduces strong easterly component (Fig. 4b) so ARs are most frequent over northwestern Pacific. Due to the modulation by the seasonally varying background moisture flux, AR frequency in the west coast of North America differs significantly between winter and summer.

c. Variability with MJO phases

In this subsection, we address the variability of background DIVT with MJO phases and its implications to variability of the AR frequency. To this end, composites of the deviations of background DIVT from the annual mean climatology for the eight Wheeler and Hendon (2004) RMM phases are constructed. Similar analysis is performed on the AR frequencies. Figure 5 shows the annual mean anomalous DIVT (arrows) and anomalous AR frequency (shadings) at each MJO phase.

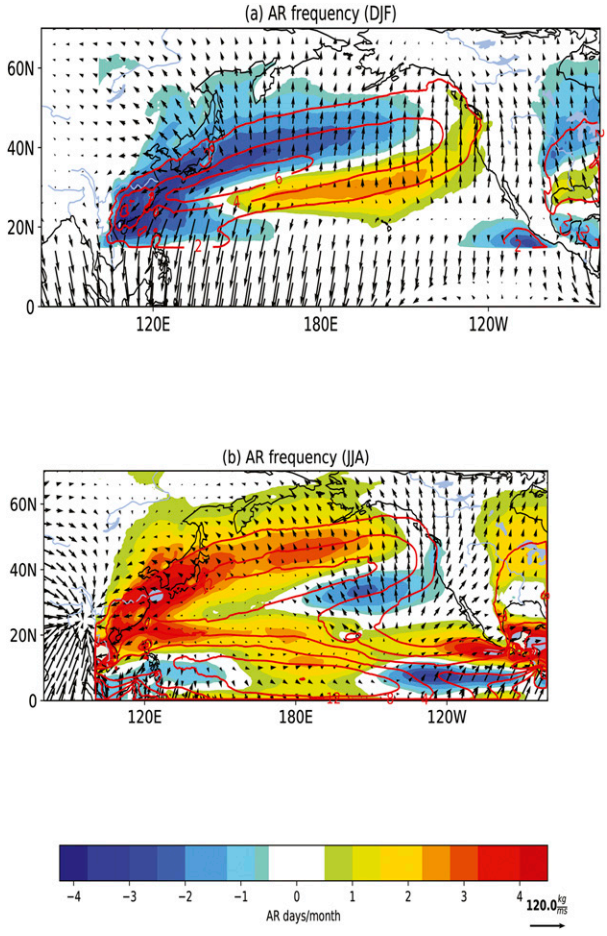

FIG. 4. The AR frequency deviations (shading) from the climatological mean (red contours) and the background DIVT (arrows) in boreal (a) winter and (b) summer. Only AR frequency anomalies that are statistically significant at the 95% confidence level are shaded.

In phase 1 and phase 2, the background DIVT is southerly and therefore AR frequencies are shifted poleward; in phases 3 and 4, the background DIVT is easterly and the zonal reach of the ARs is limited to the western Pacific. In phases 5 and 6, the moisture transport is equatorward. Last, in phases 7 and 8 the background DIVT is eastward and ARs extend furthest eastward to potentially make landfall over the western United States. Thus, the relationship of the background DIVT with the MJO can be summarized as an anticlockwise rotation of the background DIVT vector and AR frequency location with the eastward propagation of MJO moisture convergence from the Indian Ocean to the central Pacific. This can be seen in Fig. 6, which shows the anomalous contribution of the background to IVT within ARs as a function of the MJO phases.

d. Relationship to ENSO

The influence of ENSO on the spatial distribution of ARs is also examined in the moisture divergence framework. Figure 7 shows the composite spatial maps of annual mean anomalous

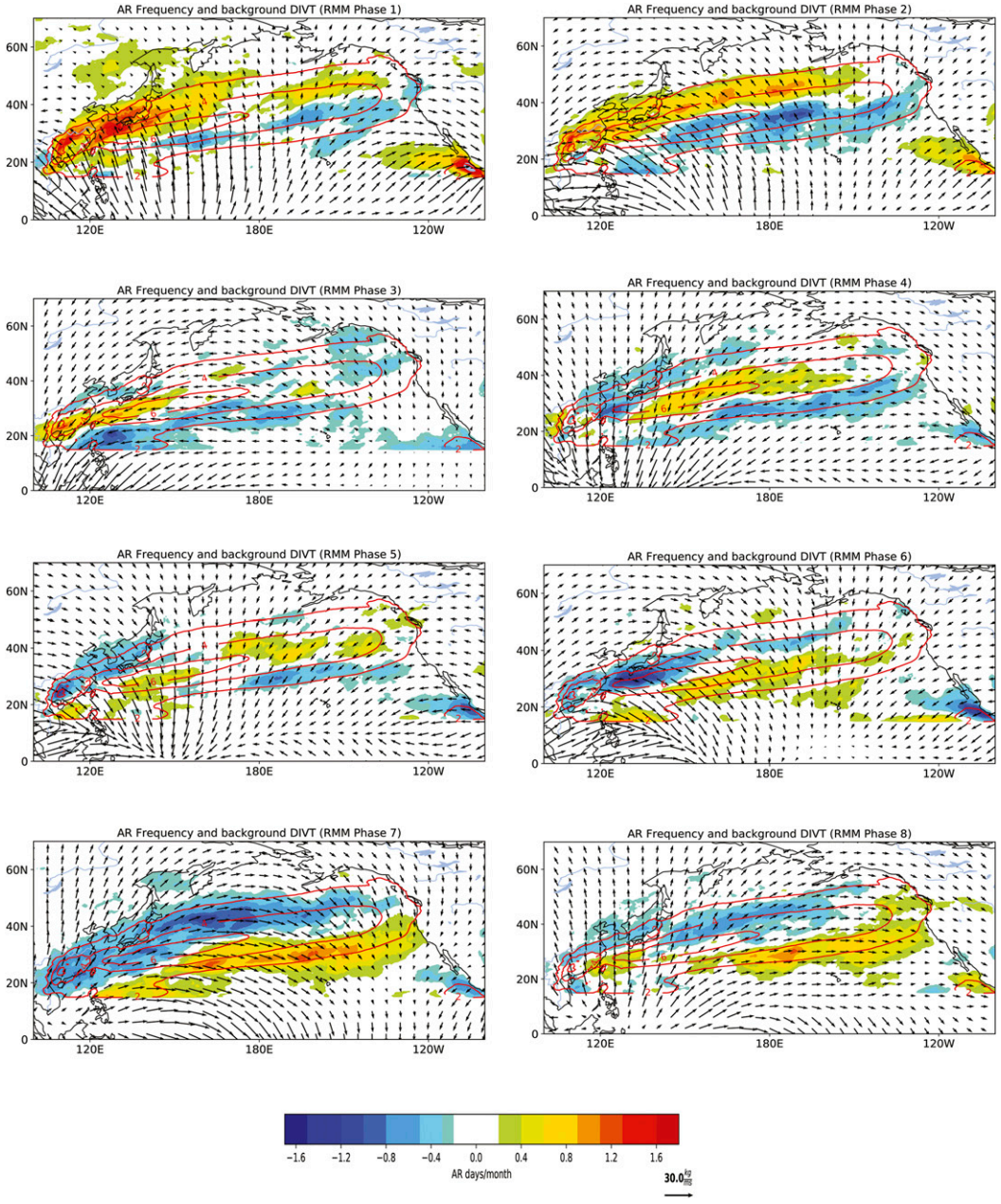

FIG. 5. The AR frequency deviations (shading) from the climatological mean (contours) and background DIVT (arrows) for the eight MJO RMM phases. Only AR frequency anomalies that are statistically significant at the 95% confidence level are shaded.

DIVT associated with each phase of ENSO as defined above. During La Niña, the moisture flux convergence center is located over northeastern Australia and eastern Maritime Continent. This convergence center shifts to the central and eastern Pacific during the different phases of El Niño. In conjunction with the change in convergence, the zonal component of DIVT over the northern Pacific shifts from easterly during La Niña to weak westerly during Modoki and stronger westerly during strong and extreme El Niño. The implication of this variability in DIVT with ENSO phases on the distribution of ARs follows from the contribution of the background DIVT to ARs. Figure 8 shows the variations of spatial distribution of ARs with the ENSO phases overlaid on the anomalous background DIVT. During La Niña, the easterly anomalous DIVT favors a westward shift of ARs, while during strong and extremely strong El Niño, the background DIVT is westerly, increasing the likelihood of ARs making landfall in the western coast of the United States. The landfalling AR response to

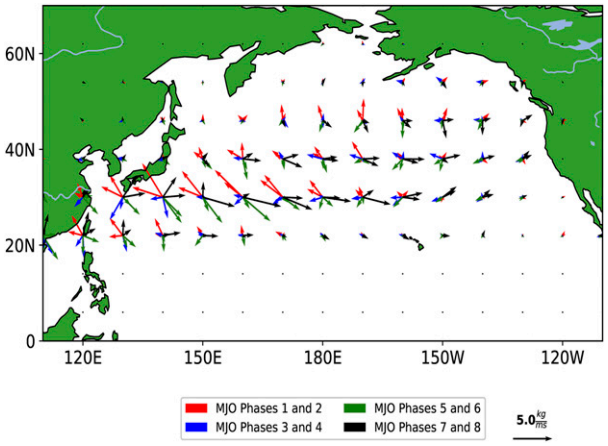

FIG. 6. The contribution of MJO-related background DIVT anomalies within AR objects. The colors correspond to the eight MJO phases and mark the counterclockwise rotation of this contribution with the phases.

ENSO is not symmetric about the ENSO phase, and that landfalling AR frequency anomalies are small for strong El Niño, with extreme El Niño needed for substantial landfalling AR anomalies (Fig. 8). This is consistent with the western U.S. precipitation response to ENSO in climate models and observations (Patricola et al. 2020). Last, it is interesting to note that during the strong El Niño year of 2016, the background DIVT turn north well before hitting the U.S. West Coast, in contrast to the 1983 and 1998 extreme El Niño years with no such turning (Fig. 6 in the online supplemental material). The difference in background DIVT contributes to the contrast in landfalling AR frequency anomalies between extreme and strong El Niño years, but understanding what influences the background IVT during extreme and strong El Niño years is beyond the scope of this study.

4. Implications for AR monitoring

In the last section, we examine the effects of the seasonal cycle, MJO, and ENSO on the spatial distribution of AR frequency through their influence on the variability of the background divergent moisture flux. Similar analysis can be performed to assess the roles of other modes of variability such as QBO and Pacific–North American (PNA). While the degree to which each of these modes affect ARs individually is of interest, even more important is their combined impacts and their values for monitoring the likelihood of AR landfall. It was shown in the last section that the modes of variability primarily impact AR frequency through their zonal component of DIVT. Therefore, we evaluate the correlation between the monthly averaged background zonal DIVT with the frequency of AR landfall. Both quantities are averaged monthly to filter out synoptic variability involving extratropical cyclones since our focus is on low-frequency variability. An AR event is assumed to have made landfall over the U.S. West Coast if at least one grid point within the AR mask is located over land between 32° and 48°N.

Figure 9a shows the map of the correlation between monthly averaged zonal background DIVT and the number of AR landfall days in that month. Only correlations with p value less than 0.01 or the 99% confidence level are shaded. The largest positive correlation values are over northeastern Pacific, just south of Alaska. There is also significant negative correlation over eastern subtropical Pacific. This indicates ARs that are most likely to make landfall on the U.S. West Coast obtain their moisture from the region immediately to their northwest and southeast. Figure 9b shows the correlation of AR landfall frequency with the background DIVT averaged over the region within the green box demarking the region enclosed by 40°–55°N, 160°–135°W. The correlation with the average zonal background DIVT value in the box is 0.75. Thus, we use that box to define an index called AR background index—a normalized index that provides a measure of the favorability of the background state for AR landfall over the United States as

$$\text{AR Background Index} = \frac{\text{DIVT}_{\text{ZBG}} - \text{mean}(\text{DIVT}_{\text{ZBG}})}{\text{std}(\text{DIVT}_{\text{ZBG}})},$$

where DIVT_{ZBG} is the background zonal DIVT of a particular month and $\text{mean}(\text{DIVT}_{\text{ZBG}})$ is the long-term-mean background zonal DIVT over all months. The index incorporates variabilities at different time scales discussed in this study (seasonality, MJO and ENSO) as well as any other low-frequency variability that can potentially affect AR landfall, excluding synoptic extratropical disturbances that are filtered out in the monthly averaging. One can also interpret this relationship as a result of modulation of storm tracks. However the background moisture flux is more general as it is a product of the wind and the moisture. Thus, the jet variability associated movement of the storm tracks are already included in the variability moisture flux. The divergent component in effect extracts the part of the jet that is responsible for the net transport of moisture while excluding the part that only contributes to the rotational component that does not actually transport moisture.

Finally, we examine the relative contributions of seasonal cycle, MJO and ENSO related variabilities in the zonal background moisture flux within ARs and how they vary with latitude. Figure 10 shows the latitudinal cross section of the zonal background DIVT averaged over the width of the box in Fig. 9a, that is, between 160° and 135°W. The variability associated with seasonal cycle is strongest (about three times that associated with MJO phases) and extends to a higher latitude (between 35° and 45°N) than that of ENSO with peak variability between 25° and 35°N. However, when present, ENSO anomalies introduce variability in the background DIVT that is comparable to that of seasonal cycle.

5. Conclusions

Understanding the mechanisms of variability of ARs and ultimately improving prediction of their landfall and impacts is of scientific and socioeconomic interest. Hence there has been considerable effort in identifying the relationship between large-scale modes of variability and ARs. This work aims to

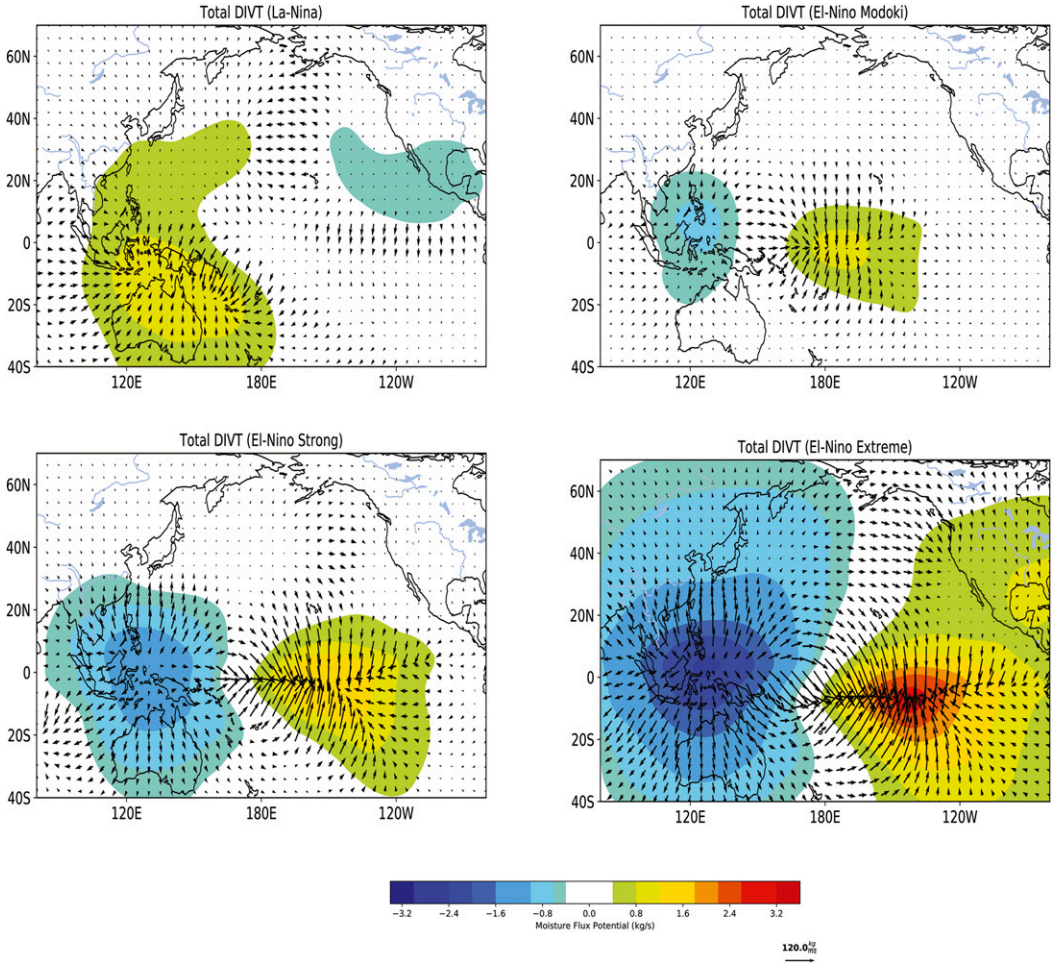

FIG. 7. The anomalous total DIVT (arrows) and moisture flux potential (shading) associated with the four ENSO phases identified using the ELI index of Williams and Patricola (2018).

offer physical explanations for the well-documented seasonality and variability of AR frequency. Since northern Pacific ARs are part of the global hydrological cycle that includes monsoonal circulations in summer as well as outflows from subtropical subsidence in winter, their variability is to some degree governed by the effect of the various modes of variability on the overall hydrological cycle. This work focuses on identifying the sources of the moisture for North Pacific ARs and quantitatively assess how different modes of variability modulate these sources. To this end, the total IVT within ARs identified using the TEMPEST algorithm as part of the ARTMIP project is partitioned into its divergent and nondivergent components. It is shown that while the former is responsible for the net transport of moisture across a closed loop of moisture flux streamfunction, the latter is associated with the channeling of the moisture flux into the signature of narrow filament of ARs notable from satellite observations but with net zero moisture flux transport. Another important nature of the divergent component of IVT is that it is related to the local (within the AR object) and nonlocal (background) moisture divergence field. In turn, the latter is related to global precipitation and evaporation patterns through conservation of moisture. Therefore, IVT in ARs is affected by the variabilities of the background moisture transport.

It is shown that ARs constitute a large fraction of the total DIVT associated with outflow from the subtropical subsidence region over northeastern Pacific during winter as well as the monsoonal southeasterly flux during summer (Fig. 3). Thus, as part of this seasonal monsoonal circulation ARs migrate northwestward in boreal summer and southeastward in winter as documented by Mundhenk et al. (2016). Another large-scale factor that has been shown to affect AR variability is the MJO (Guan et al. 2012). In this work we provide a quantitative assessment of the modulation of the background moisture flux and hence the spatial distribution of ARs by MJO propagation. As the anomalous moisture convergence field associated with the MJO moves eastward from equatorial Indian Ocean and across the Maritime Continent and Pacific, the associated moisture flux divergence over northern Pacific shows an anticlockwise rotation starting from southerly in MJO RMM phases

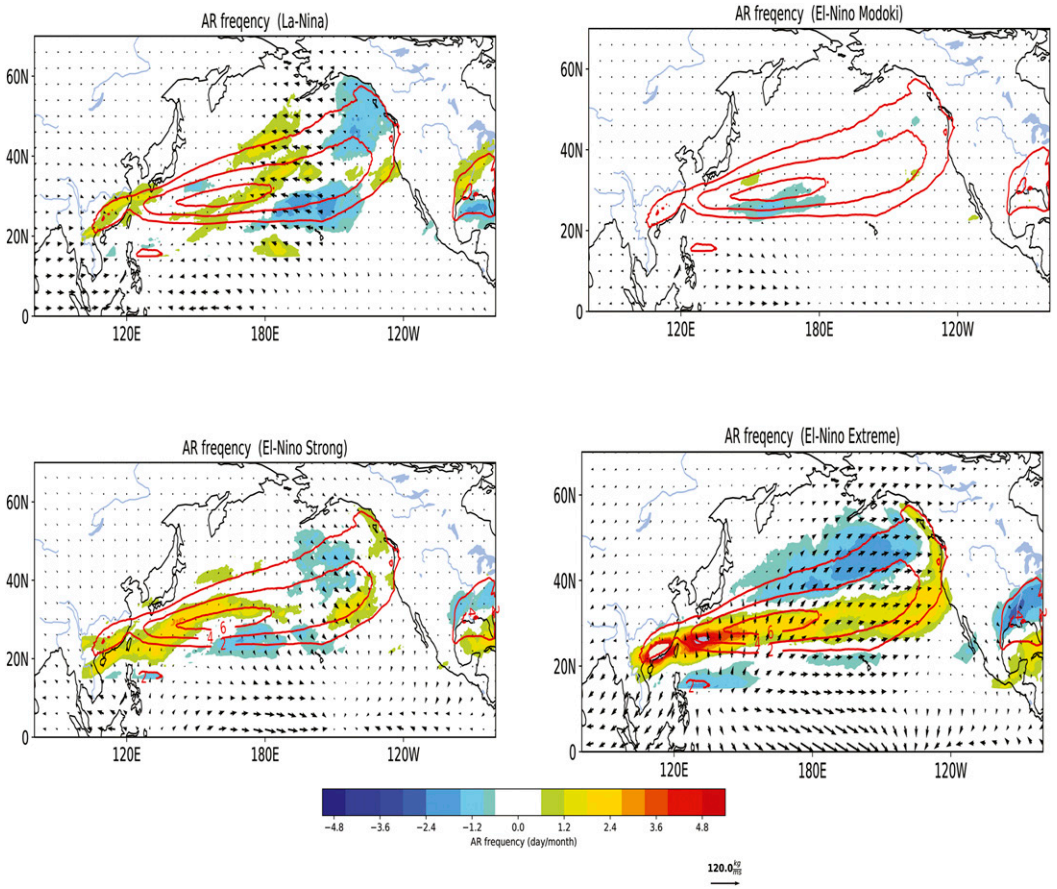

FIG. 8. The AR frequency anomalies (shading), climatological mean (contours), and background DIVT (arrows) for the four ENSO phases. Only AR frequency anomalies that are statistically significant at the 95% confidence level are shaded.

1 and 2, to easterly during phases 3 and 4, to northerly during 5 and 6 and to westerly during phases 7 and 8. The frequency of ARs follows this background DIVT pattern such that ARs are most likely to make landfall over the West Coast of the United States during the last two phases. At interannual scales, ENSO affects AR frequency in a similar manner. During La Niña, the background DIVT is easterly while during strong and extremely strong El Niño events the direction is reversed and ARs are more likely to make landfall (Fig. 7), leading to increased precipitation over the West Coast of the United States as noted in Patricola et al. (2020).

One key feature of the effect of background DIVT, which varies over a broad range of scales, is that its primary effect on ARs is additive and thus instead of using multiple indices such as ENSO ELI and MJO–RMM to describe the background state, one can calculate the direction and magnitude of this background DIVT in a certain region that is most relevant to the likelihood of AR landfall. In this work we define a background AR index that reflects the state of the background DIVT within a box over the northern Pacific region for monitoring the likelihood of landfall over the United States. The impact of seasonality, MJO, and ENSO on AR landfalling frequency is summarized by the meridional distribution of the background IVT contributed by each mode of variability (Fig. 10). Compared to seasonality, the impact of MJO and ENSO is generally smaller except during extreme El Niño events.

This study focuses on the low-frequency large-scale environmental condition and less on synoptic-scale processes involving extratropical cyclones, which are important for understanding the dynamics of ARs and improving AR forecasts. In our results, the frequency of ARs is taken from the ARTMIP data based on a single AR tracking algorithm (TEMPEST). As AR frequency is rather sensitive to the detection algorithm, using AR frequency from a single algorithm may introduce uncertainty in our analysis. Repeating our analysis using AR frequency taken from ARTMIP associated with another AR tracking algorithm (supplemental Figs. 1–3), we demonstrate the robustness of our findings. It should also be noted that the variabilities of AR frequencies at seasonal, intraseasonal, and interannual scales are well documented in previous studies in which ARs were tracked using several other algorithms. While the influence of seasonality, MJO, and ENSO on ARs has already been documented in the

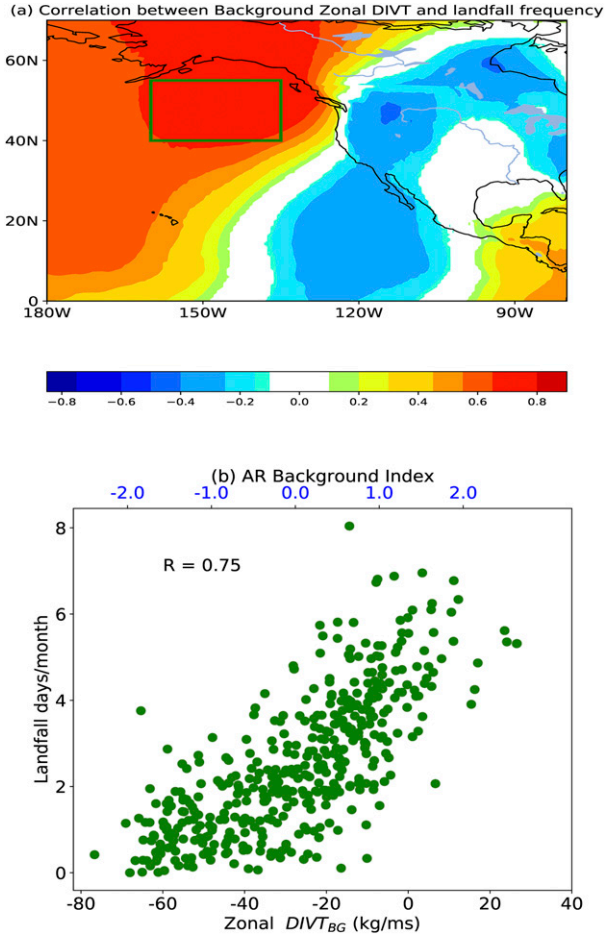

FIG. 9. (a) The correlation between monthly averaged zonal background DIVT with the number of AR landfall days over the U.S. West Coast. (b) The relationship between the number of AR landfall days and the monthly mean zonal background DIVT averaged over the green box in (a). The zonal DIVT is normalized to define the ''AR background index'' for monitoring applications; see the top axis of (b).

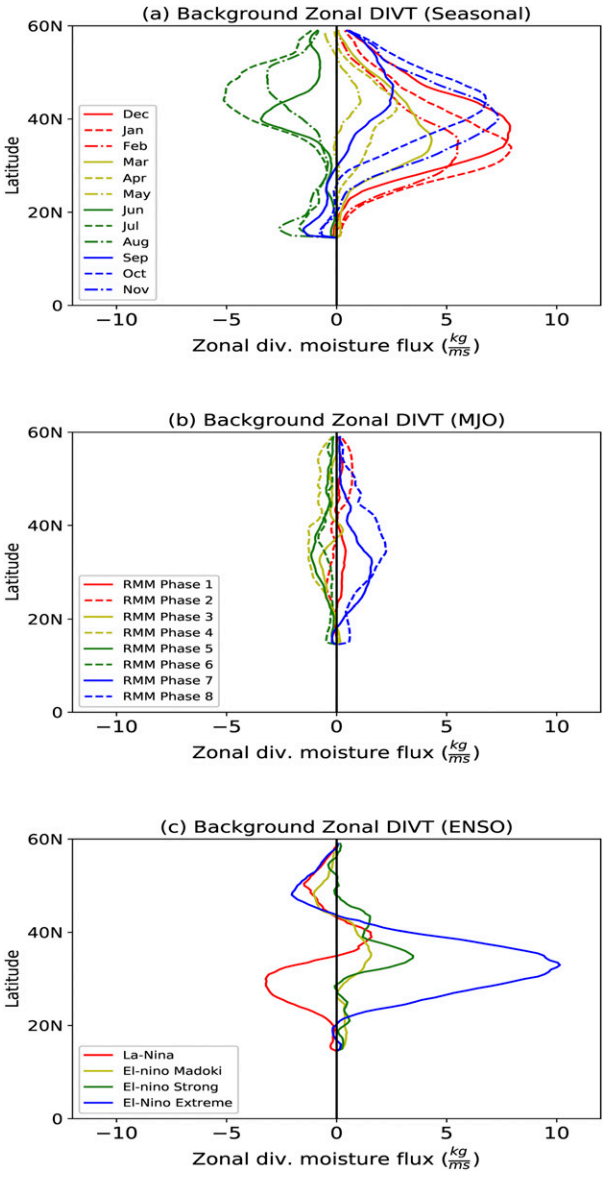

FIG. 10. The meridional structure of the variability background zonal DIVT with (a) seasonal cycle, (b) MJO phases, and (c) ENSO phases averaged over the width of the box in Fig. 9a.

literature, this study highlights the modulation of the background moisture transport in connecting the modes of variability with AR IVT and landfalling frequency. In a future work we will examine the implications of the relationship between the background divergent moisture flux and AR frequency revealed in this study for the response of ARs and associated distribution of extreme precipitation to anthropogenic global warming.

Acknowledgments. This work is supported by U.S. Department of Energy Office of Science Biological and Environmental Research as part of Global and Regional Model Analysis program area. The contribution of YG is supported by National Oceanic and Atmospheric Administration (NOAA) Oceanic and Atmospheric Research, Program Climate Program Office (CPO), under NOAA Grant NA17OAR4310263. ARTMIP is a grass-roots community effort and includes a collection of international researchers from universities, laboratories, and agencies. Co-chairs and committee members include Jonathan Rutz, Christine Shields, L. Ruby Leung, F. Martin Ralph, and Michael Wehner. Details on catalogs developers can be found on the ARTMIP website. ARTMIP has received support from the U.S. Department of Energy Office of Science Biological and Environmental Research (BER) as part of the Regional and Global Model Analysis program area, and the Center for Western Weather and Water Extremes (CW3E) at Scripps Institute for Oceanography at the University of California, San Diego. Computing resources for the analysis are provided by the National Energy Research

Scientific Computing Center (NERSC). Pacific Northwest National Laboratory is operated by Battelle for the U.S. Department of Energy under Contract DE-AC05-76RLO1830. Lawrence Berkeley National Laboratory is managed by the University of California for the U.S. Department of Energy under Contract DE-AC02-05CH11231.

REFERENCES

Bao, J.-W., S. A. Michelson, P. J. Neiman, F. M. Ralph, and J. M. Wilczak, 2006: Interpretation of enhanced integrated water vapor bands associated with extratropical cyclones: Their formation and connection to tropical moisture. *Mon. Wea. Rev.*, **134**, 1063–1080, https://doi.org/10.1175/MWR3123.1.

Dacre, H. F., P. A. Clark, O. Martinez-Alvarado, M. A. Stringer, and D. A. Lavers, 2015: How do atmospheric rivers form? *Bull. Amer. Meteor. Soc.*, **96**, 1243–1255, https://doi.org/10.1175/BAMS-D-14-00031.1.

Dettinger, M. D., 2013: Atmospheric rivers as drought busters on the U.S. West Coast. *J. Hydrometeor.*, **14**, 1721–1732, https://doi.org/10.1175/JHM-D-13-02.1.

——, F. M. Ralph, T. Das, P. J. Neiman, and D. Cayan, 2011: Atmospheric rivers, floods, and the water resources of California. *Water*, **3**, 455–478, https://doi.org/10.3390/w3020445.

Gershunov, A., T. Shulgina, F. M. Ralph, D. Lavers, and J. J. Rutz, 2017: Assessing the climate-scale variability of atmospheric rivers affecting the west coast of North America. *Geophys. Res. Lett.*, **44**, 7900–7908, https://doi.org/10.1002/2017GL074175.

Guan, B., and D. E. Waliser, 2015: Detection of atmospheric rivers: Evaluation and application of an algorithm for global studies. *J. Geophys. Res.*, **120**, 12 514–12 535, https://doi.org/10.1002/2015JD024257.

——, ——, N. P. Molotch, E. J. Fetzer, and P. J. Neiman, 2012: Does the Madden–Julian oscillation influence wintertime atmospheric rivers and snowpack in the Sierra Nevada? *Mon. Wea. Rev.*, **140**, 325–342, https://doi.org/10.1175/MWR-D-11-00087.1.

Guirguis, K., A. Gershunov, R. E. S. Clemesha, T. Shulgina, A. C. Subramanian, and F. M. Ralph, 2018: Circulation drivers of atmospheric rivers at the North American west coast. *Geophys. Res. Lett.*, **45**, 12576–12584, https://doi.org/10.1029/2018GL079249.

Leung, L. R., and Y. Qian, 2009: Atmospheric rivers induced heavy precipitation and flooding in the western U.S. simulated by the WRF regional climate model. *Geophys. Res. Lett.*, **36**, L03820, https://doi.org/10.1029/2008GL036445.

Mundhenk, B. D., E. A. Barnes, and E. D. Maloney, 2016: All-season climatology and variability of atmospheric river frequencies over the North Pacific. *J. Climate*, **29**, 4885–4903, https://doi.org/10.1175/JCLI-D-15-0655.1.

Neiman, P. J., F. M. Ralph, G. A. Wick, J. D. Lundquist, and M. D. Dettinger, 2008: Meteorological characteristics and overland precipitation impacts of atmospheric rivers affecting the west coast of North America based on eight years of SSM/I satellite observations. *J. Hydrometeor.*, **9**, 22–47, https://doi.org/10.1175/2007JHM855.1.

Patricola, C. M., J. P. O'Brien, M. D. Risser, A. M. Rhoades, T. A. O'Brien, P. A. Ullrich, D. A. Stone, and W. D. Collins, 2020: Maximizing ENSO as a source of western US hydroclimate predictability. *Climate Dyn.*, **54**, 351–372, https://doi.org/10.1007/s00382-019-05004-8.

Payne, A. E., and G. Magnusdottir, 2014: Dynamics of landfalling atmospheric rivers over the North Pacific in 30 years of MERRA reanalysis. *J. Climate*, **27**, 7133–7150, https://doi.org/10.1175/JCLI-D-14-00034.1.

Ralph, F. M., P. J. Neiman, G. A. Wick, S. I. Gutman, M. D. Dettinger, D. R. Cayan, and A. B. White, 2006: Flooding on California's Russian River: Role of atmospheric rivers. *Geophys. Res. Lett.*, **33**, L13801, https://doi.org/10.1029/2006GL026689.

Rutz, J. J., W. J. Steenburgh, and F. M. Ralph, 2014: Climatological characteristics of atmospheric rivers and their inland penetration over the western United States. *Mon. Wea. Rev.*, **142**, 905–921, https://doi.org/10.1175/MWR-D-13-00168.1.

——, and Coauthors, 2019: The Atmospheric River Tracking Method Intercomparison Project (ARTMIP): Quantifying uncertainties in atmospheric river climatology, *J. Geophys. Res. Atmos.*, **124**, 13777–13802, https://doi.org/10.1029/2019JD030936.

Ryoo, J.-M., Y. Kaspi, D. W. Waugh, G. N. Kiladis, D. E. Waliser, E. J. Fetzer, and J. Kim, 2013: Impact of Rossby wave breaking on U.S. West Coast winter precipitation during ENSO events. *J. Climate*, **26**, 6360–6382, https://doi.org/10.1175/JCLI-D-12-00297.1.

Shields, C. A., and Coauthors, 2018: Atmospheric River Tracking Method Intercomparison Project (ARTMIP): Project goals and experimental design. *Geosci. Model Dev.*, **11**, 2455–2474, https://doi.org/10.5194/gmd-11-2455-2018.

Sodemann, H., and A. Stohl, 2013: Moisture origin and meridional transport in atmospheric rivers and their association with multiple cyclones. *Mon. Wea. Rev.*, **141**, 2850–2868, https://doi.org/10.1175/MWR-D-12-00256.1.

Ullrich, P. A., and C. M. Zarzycki, 2017: TempestExtremes: A framework for scale-insensitive pointwise feature tracking on unstructured grids. *Geosci. Model Dev.*, **10**, 1069–1090, https://doi.org/10.5194/gmd-10-1069-2017.

Waliser, D. E., and B. Guan, 2017: Extreme winds and precipitation during landfall of atmospheric rivers. *Nat. Geosci.*, **10**, 179–183, https://doi.org/10.1038/ngeo2894.

Wheeler, M. C., and H. H. Hendon, 2004: An all-season Real-Time Multivariate MJO Index: Development of an index for monitoring and prediction. *Mon. Wea. Rev.*, **132**, 1917–1932, https://doi.org/10.1175/1520-0493(2004)132<1917:AARMMI>2.0.CO;2.

Williams, I. N., and C. M. Patricola, 2018: Diversity of ENSO events unified by convective threshold sea surface temperature: A nonlinear ENSO index. *Geophys. Res. Lett.*, **45**, 9236–9244, https://doi.org/10.1029/2018GL079203.

Zhou, Y., H.-M. Kim, and B. Guan, 2018: Life cycle of atmospheric rivers: Identification and climatological characteristics. *J. Geophys. Res. Atmos.*, **123**, 12715–12725, https://doi.org/10.1029/2018JD029180.

Zhu, Y., and R. E. Newell, 1998: A proposed algorithm for moisture fluxes from atmospheric rivers. *Mon. Wea. Rev.*, **126**, 725–735, https://doi.org/10.1175/1520-0493(1998)126<0725:APAFMF>2.0.CO;2.